Available online at www.sciencedirect.com
ScienceDirect
Applied Catalysis B: Environmental 79 (2008) 186–198
APPLIED CATALYSIS B: ENVIRONMENTAL
www.elsevier.com/locate/apcatb

$LaMO_3$ (M = Mg, Ti, Fe) perovskite type oxides: Preparation, characterization and catalytic properties in methane deep oxidation

S. Petrović [a,*], A. Terlecki-Baričević [a], Lj. Karanović [b], P. Kirilov-Stefanov [c], M. Zdujić [d], V. Dondur [e], D. Paneva [f], I. Mitov [f], V. Rakić [g]

[a] *ICTM – Department of Catalysis and Chemical Engineering, Njegoševa 12, 11000 Belgrade, Serbia*
[b] *Laboratory for Crystallography, Faculty of Mining and Geology, University of Belgrade, Đušina 7, 11000 Belgrade, Serbia*
[c] *Institute of General and Inorganic Chemistry, Bulgarian Academy of Sciences, 1040 Sofia, Bulgaria*
[d] *Institute of Technical Sciences of SASA, Knez Mihailova 35, 11000 Belgrade, Serbia*
[e] *Faculty of Physical Chemistry, P.O. Box 137, 11000 Belgrade, Serbia*
[f] *Institute of Catalysis, Bulgarian Academy of Sciences, 1113 Sofia, Bulgaria*
[g] *Faculty of Agriculture, Nemanjina 6, Zemun, P.O. Box 127, 11081 Belgrade, Serbia*

Received 22 June 2007; received in revised form 16 October 2007; accepted 21 October 2007
Available online 26 October 2007

Abstract

Two new series of perovskite-type oxides $LaMO_3$ (M = Mg, Ti, Fe) with different ratio Mg/Fe (MF) and Ti/Fe (TF) in the B cation site were prepared by annealing the precursor, obtained by the mechanochemical activation (MCA) of constituent metal oxides, at 1000 °C in air. In addition, two closely related perovskites $LaFeO_3$ (LF) and $LaTi_{0.5}Mg_{0.5}O_3$ (TM (50:50)) were synthesized in the similar way. Using MCA method, perovskites were obtained in rather short time and at room temperature. The samples were characterized by X-ray powder diffraction (XRPD), X-ray photoelectron spectroscopy (XPS), scanning electron microscopy (SEM) with energy dispersive X-ray spectroscopy (EDS), temperature programmed desorption of oxygen (TPD), Mössbauer spectroscopy, BET surface area measurements and tested in methane deep oxidation. According to XRPD analysis all synthesized samples are almost single perovskite phase, with trace amounts of La_2O_3 phase. Data of Mössbauer spectroscopy identify Fe^{3+} in octahedral coordination. The activity of perovskite in methane deep oxidation increases in the order TM (50:50) < MF series < TF series. Higher activity of TF samples in respect to MF with similar Fe content can be related to the structural characteristic, mainly to the presence of predominantly most labile oxygen species evidenced by TPD at lowest temperature of oxygen evaluation. In used experimental conditions, the Fe substituted perovskite are thermal stable up to the temperature of 850 °C. The stability of Fe active sites is probably the most important parameter responsible for thermal stability of perovskite, but the atomic surface composition also should be taken into account.

Keywords: Perovskite catalysts; Catalyst characterization; Methane combustion

1. Introduction

Many materials show an interesting activity in methane oxidation but very few of them sustain the operation at high temperatures. Depending of the design of the catalytic combustion system catalysts are exposed to a wide range of temperatures extending from 500 to 1300 °C, not less than 900 °C.

Perovskite oxides with general formula ABO_3 provide excellent catalytic activity and thermal stability for hydrocarbon oxidation [1,2]. They can be easily prepared by the partial substitution of A and B cation sites by third one. This substitution usually modifies the catalytic properties, very often by influencing oxygen availability [3,4].

Various methods of preparation were used for the synthesis of perovskite: ceramic [5,6], spray drying [7], sol–gel and citrate method [8–14], thermal decomposition of nitrate mixtures [15–19], combustion synthesis [20–22], etc. However, the literature data show that it is not easy to keep the high surface area and to avoid sintering processes simultaneously in those procedures.

* Corresponding author. Tel.: +381 11 2630213; fax: +381 11 2637977.
E-mail address: srlepp@gmail.com (S. Petrović).

0926-3373/$ – see front matter © 2007 Elsevier B.V. All rights reserved.
doi:10.1016/j.apcatb.2007.10.022

Recently the mechanochemical activation was widely used as a method for preparation of various types of materials [23]. Many complex, multi-component metallic and ceramic materials which may be otherwise difficult to synthesize by conventional high temperature treatment, have been successfully prepared by intensive milling. Kaliaguine et al. [24] and Szabo et al. [25–27] reported the synthesis of $LaCoO_3$ and $LaCo_xFe_{1-x}O_3$ perovskites by mechanochemical treatment of the mixture of appropriate reactants and additives.

The results of our previous studies [28,29] of the phase composition and surface properties of binary (La_2O_3–MgO, La_2O_3–TiO_2, TiO_2–MgO and MgO–PdO) and ternary (La_2O_3–TiO_2–MgO) mixtures obtained by mechanochemical activation points out the affinity of constituent oxides to the formation of perovskite-type structures. The methane oxidation activity of single-phase $LaMg_{0.5}TiO_{0.5}O_3$ prepared by MCA was higher than the activity of the sample synthesized by ceramic method. The specific surface area of both samples was around 5 m^2/g. Since the milling of constituent oxides was performed with hardened steel balls and vial, some iron contamination was observed in the final product. Consequently, the reason for higher activity can be ascribed to the incorporation of Fe ions in the perovskite structure. Following that, perovskite with nominal formula $LaTi_{0.4}Mg_yFe_xO_3$ ($0.2 \leq x \leq 0.4$; $0.1 \leq y \leq 0.4$) and $LaMg_{0.5}Ti_yFe_xO_3$ ($0.13 \leq x \leq 0.53$; $0.1 \leq y \leq 0.4$) as well as $LaFeO_3$ and $LaTi_{0.5}Mg_{0.5}O_3$ were synthesized by annealing mechanochemically prepared samples as a precursor. This work was undertaken with the aim to follow the effect of iron substitution in $LaTi_{0.5}Mg_{0.5}O_3$ in methane deep oxidation. Characterization of catalyst structure was performed by XRPD, XPS, SEM–EDS, TPD analysis, Mössbauer spectroscopy, SSA measurements in order to correlate surface and bulk properties with catalytic activity.

In the second part of this paper the kinetic of methane oxidation will be discussed with the aim to elucidate the role of the state and degree of Fe substitution.

2. Experimental

MCA was used to prepare the following mixed oxides: $LaFeO_3$, $LaTi_{0.5}Mg_{0.5}O_3$, $LaTi_{0.4}Mg_yFe_xO_3$ ($0.2 \leq x \leq 0.4$; $0.1 \leq y \leq 0.4$) and $LaMg_{0.5}Ti_yFe_xO_3$ ($0.13 \leq x \leq 0.53$; $0.1 \leq y \leq 0.4$). The samples are designated according the following notations and presented in Table 1.

Appropriate amounts of La_2O_3 (99.99%), MgO (96%), TiO_2 (99%) and Fe_2O_3 (99.5%) were mixed. All used chemicals are produced by Johnson Matthey GMBH Alfa Aesar. The mixture was intensively milled for 1 h in planetary ball mill Fritsh Pulverisette 5 under the following conditions: air atmosphere, hardened-steel vials of 500 cm^3 volume, hardened-steel balls of a diameter 13.4 mm, mass of the powder 10 g, ball to powder weight ratio of 30: 1, basic disc rotation speed 317 rpm, disc with vials rotation speed 396 rpm. Prepared precursor was annealed at 1000 °C in air for 10 h. The specific surface area (SSA) of the samples was determined by BET method at the temperature of liquid nitrogen using Thermo Finnigan Sorptomatic 1990 series. Apparatus provides the measurement of the surface area as small as 0.2 m^2/g in the sample cell, with an error of ±5%.

Table 1
The notation and nominal composition of samples

Notation	Nominal composition
TM (50:50)	$LaTi_{0.5}Mg_{0.5}O_3$
MF series	
MF (40:20)	$LaTi_{0.4}Mg_{0.4}Fe_{0.2}O_3$
MF (30:27)	$LaTi_{0.4}Mg_{0.3}Fe_{0.27}O_3$
MF (20:34)	$LaTi_{0.4}Mg_{0.2}Fe_{0.34}O_3$
MF (10:40)	$LaTi_{0.4}Mg_{0.1}Fe_{0.4}O_3$
TF series	
TF (40:13)	$LaMg_{0.5}Ti_{0.4}Fe_{0.13}O_3$
TF (30:27)	$LaMg_{0.5}Ti_{0.3}Fe_{0.27}O_3$
TF (20:40)	$LaMg_{0.5}Ti_{0.2}Fe_{0.4}O_3$
TF (10:53)	$LaMg_{0.5}Ti_{0.1}Fe_{0.53}O_3$
LF	$LaFeO_3$

XRPD analysis was used to identify the crystal phases. The powder diffraction data were collected at room temperature using a Philips PW 1710 diffractometer in a Bragg–Brentano geometry with a curved graphite monochromator, Cu Kα radiation (λ = 1.5418 Å) and step-scan mode (range: 4–90° 2θ, step-time: 0.50 s, step-width: 0.02°). Program LSUCRIPC was used for calculation of unit-cell parameters [30].

The microstructure was investigated by SEM (JEOL, model JSM 6460-LV) and by EDS analysis (Oxford Instrument). The quantitative analysis of the elemental content was performed using the software INCA X-Sight. The acquisition time per location was 10 min. The SEM accelerating voltage was 25 keV. The area of spot analysis was 1 μm^2 at the site being analyzed; the scanned areas were ~60 μm × 50 μm. The elements O, La, Ti, Mg and Fe were determined by X-ray energy dispersive analysis (EDS) from their K-lines.

The valence state and atomic concentration of elements in the surface layers were determined using XPS. Measurements were performed in a VC Escalab II spectrometer using un-monochromatic Mg Kα radiation ($h\nu$ = 1253.6 eV). The base pressure of instrument was 1×10^{-10} Torr. Electrostatic surface charging was observed in all investigated samples owing to their poor electric conductivity. Therefore, C 1s with the binding energy (BE) of 285.0 eV from carbon contaminations was used as a reference level. The binding energies reported here were measured within ±0.2 eV. XPS surface compositions were calculated from photoelectron peak areas of each element after correcting for instrument parameters.

Mössbauer spectra of mechanochemically synthesised perovskite type oxides were recorded at 295 K on a Wissel electromechanical Mössbauer spectrometer (Wissenschaftliche Elektronik GmbH, Germany) working in a constant acceleration mode. A ^{57}Co/Cr (activity ≅10 mCi) source and an α-Fe standard were used. The experimental spectra were treated using the least squares method. The parameters of hyperfine interaction such as isomer shift (IS), quadrupole splitting (QS) and effective internal magnetic field (H_{eff}) as well as the line

Table 2
Nominal and surface (XPS) atomic concentrations of elements in synthesized samples

Sample	Bulk concentration (at.%)					Surface concentration (at.%)					SSA (m^2/g)
	La	Ti	Mg	Fe	O	La	Ti	Mg	Fe	O	
TM (50:50)	20.0	10.0	10.0	–	60.0	10.8	7.3	14.9	–	67.1	4.7
MF (40:20)	20.0	8.0	8.0	4.0	60.0	9.2	5.5	12.6	1.4	71.2	3.5
MF (30:27)	20.0	8.0	6.0	5.4	60.0	11.5	7.3	6.3	2.2	72.7	1.9
MF (20:34)	20.0	8.0	4.0	6.8	60.0	11.0	6.7	5.7	2.2	74.3	2.1
MF (10:40)	20.0	8.0	2.0	8.0	60.0	11.7	6.8	3.0	2.8	75.6	2.4
TF (40:13)	20.0	8.0	10.0	2.6	60.0	8.0	4.2	18.3	0.7	68.7	3.3
TF (30:27)	20.0	6.0	10.0	5.4	60.0	7.4	3.3	16.1	2.3	70.9	1.8
TF (20:40)	20.0	4.0	10.0	8.0	60.0	7.3	2.3	20.9	1.9	67.5	1.9
TF (10:53)	20.0	2.0	10.0	10.6	60.0	8.4	1.4	18.2	2.9	69.1	2.1
LF	20.0	–	–	20.0	60.0	11.0	–	–	14.9	73.2	1.8

widths (FWHM) and the relative weight (G) of the partial components of the spectra were determined.

TPD experiments were performed on a Setaram TG-DSC 111 equipment coupled with a mass spectrometer (Thermostar from Pfeiffer) as a detector; capillary-coupling system was used. The TPD experiments were carried out in a continuous flow system, ca. 200 mg of the sample was placed in a DSC furnace. All experiments were composed of two sequences, in the first one the sample was exposed to oxygen, and then in the second one the temperature programmed desorption was done under the helium flow; all steps were performed in situ. In the first sequence, the sample was flushed with oxygen at 25 °C for 10 min; then, it was heated up to 800 °C at 10 C min^{-1} and, subsequently, cooled down up to 100 °C, all time under the same (oxygen) atmosphere. The sample was flushed with helium for 1 h, and heated up to 800 °C at 10 C min^{-1}, in helium. Both oxygen and helium flow were kept at 30 ml min^{-1}. During the whole experiment, the following mass fragmentations were recorded: 17, 18, 28, 32, 44. In this way, the temperature-programmed profiles of H_2O, CO, CO_2 and O_2 were monitored.

Catalytic activity tests in methane oxidation were performed in fixed bed tubular reactor (8 mm i.d.) at the atmospheric pressure. The reactor was positioned in the electrical furnace provided by a thermocouple on its wall. The temperature of the reactor was maintained by the temperature controller. The temperature of the catalyst bed was monitoring by chromel–alumel thermocouple placed in the catalyst bed. The space velocity was 100,000 h^{-1} and a feed gas composition 1.0 vol.% CH_4, 15 vol.% O_2 and N_2 as a balance. Catalyst particles in 1.02–1.20 mm were diluted 1:1 with quartz powder with the same particle size.

The inlet and outlet gas mixture was analyzed by on-line gas chromatograph Shimadzu GC-8A, equipped with TCD detector and interfaced with an automatic integrator. Carbon dioxide was analyzed using Hayesep D column. Oxygen, nitrogen, carbon monoxide and methane were determined using Molecular sieve 13× column. The only detected gas products were O_2, CO_2 and CH_4. The mass balance with respect to carbon was 100 ± 5%. The experiments were performed during heating of samples up to 850 °C, and cooling to the temperature at which the conversion of methane was detectable. For each test the methane conversion was calculated as average of all but at least three measurements.

3. Results

3.1. Catalyst composition

The nominal atomic concentrations of elements in the bulk and these determined by XPS in the surface layers and SSA of both catalyst series annealed at 1000 °C are presented in Table 2.

Due to the presence of three elements with different valence state (Ti^{4+}, Mg^{2+} and Fe^{3+}) the content of elements in B position of perovskite phase is chosen to give a charge sum of 3+. Therefore, the ratio A/ΣB is not equal to 1 in Fe substituted samples. In these samples the appearance of nonstoichiometric perovskite phases with vacancies of A, B and/or O sites is expected, which could influence in catalytic properties of prepared materials.

The specific surface area (SSA) for Fe substituted samples slightly decreases in respect to TM (50:50) and remained almost constant (about 2 m^2/g) for the MF and TF samples with ratio higher than 30:27.

3.2. X-ray powder diffraction

XRPD patterns of the samples obtained after the mechanochemical treatment and annealing at 1000 °C are presented in Figs. 1 and 2, respectively.

Since milling induces disordering of crystal structures, the peak broadening was visible for mechanochemically treated samples. In all samples the predominant crystal phase has a cubic perovskite-type structure. The unit cell parameters in the range 3.919(3)–3.949(3) Å (Table 3.) were calculated. The only exception is the TM with $La(OH)_3$ as the main phase whereby the perovskite phase was present in a smaller amount. In addition, the existence of very disordered residual La_2O_3 (as indicated by two weak maxima in the 25–30° 2θ interval) and γ-Fe (which originates from the vial and ball debris) was confirmed. Both, La_2O_3 and γ-Fe are present in trace amounts only. In Fe-rich samples (MF (20:34), MF (10:40), TF (10:53) and LF) the appearance of two weak maxima at about 33.2 and

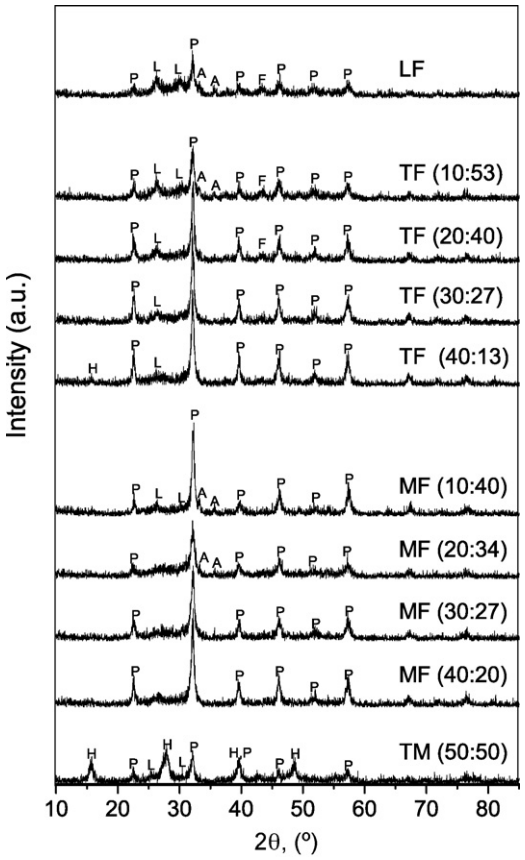

Fig. 1. The XRPD patterns of mechanochemically treated samples: P – perovskite; L – La_2O_3; A – α-Fe_2O_3; H – $La(OH)_3$; F – γ-Fe.

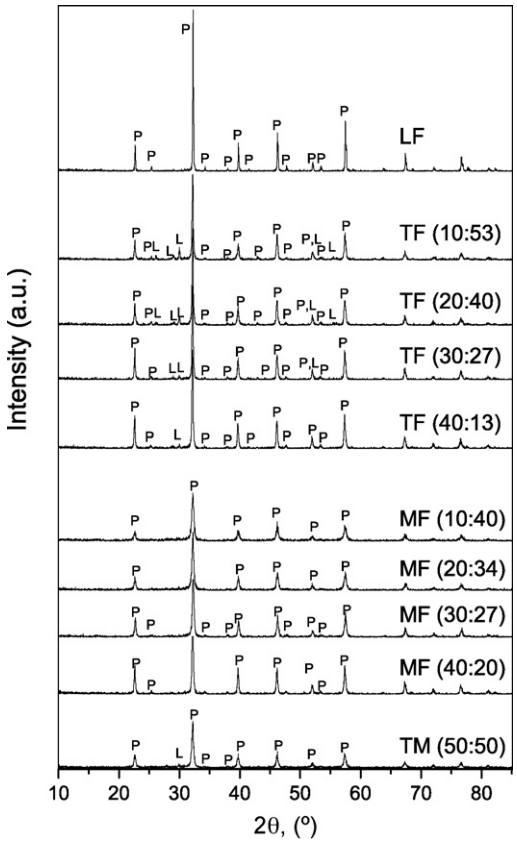

Fig. 2. XRPD patterns of the samples annealed at 1000 °C/10 h: P – perovskite; L – La_2O_3.

35.6° 2θ suggested the presence of disordered unreacted hematite (α-Fe_2O_3).

After annealing at 1000 °C the phase composition was significantly changed. Almost single-phase samples were obtained in which cubic perovskites were transformed into orthorhombic perovskite-type structures with a higher degree of crystallinity. In some annealed samples with a lower degree of crystallinity (samples MF (20:34) and MF (10:40)), it was hard to recognize the actual symmetry of the perovskite phase because the maxima associated with the orthorhombic symmetry were very weak. A trace amount of La_2O_3 was also observed in all samples, but in samples TF (20:40) and TF (10:53) the content of La_2O_3 content was slightly higher. In all cases the unit cell parameters of perovskite phases (Table 3) are similar and correspond well to the literature data for perovskites with comparable chemical compositions, like $La(Mg_{0.5}Ti_{0.5})O_3$ [31] $La_{0.834}(Ti_{0.4}Fe_{0.6})O_3$ [32] and $LaFeO_3$ [33].

It seems that perovskites of the annealed samples could be classified in two groups: one with unit cell volumes $V = 241.9(3)$–$242.6(1)$ Å^3 and another with $V = 243.0(1)$–$243.4(1)$ Å^3. Within each group the variations of the unit cell volumes are in the range from one to three standard deviations. For the first group the nominal contents are Fe $\geq$ 0.27 and Ti + Mg is $\leq$0.8. The variation of unit cell parameters, and consequently of unit cell volumes, could be a result of different amounts of Fe, Mg and Ti in the octahedral site, their valence states, possible cation and oxygen vacancies and the different degree of distortion of octahedral alignment (i.e. octahedral tilting about a single pseudo cubic axis) [34–36].

3.3. SEM–EDS

SEM images of the samples with lowest and highest degree of substitution are presented in Fig. 3.

The SEM images (Fig. 3) show that all samples annealed at 1000 °C consist mainly of large particles. The average density of the powders of all samples measured by pycnomectric method was 5.06 g/cm^3. From this result and SSA the grain size was calculated [37]. Assuming spherical geometry, the obtained grain radius varies in the range 0.17–0.29 μm, and the calculated grain size was around 0.34–0.60 μm. The ratios between each element and the sum of elements (La + Ti + Mg + Fe) obtained by EDS and calculated according nominal composition are compared in the Table 4.

The ratio between the each element and sum of elements detected from EDS is the same or very close to the nominal one. This implies that the distribution of elements in the bulk is almost homogeneous.

3.4. Mössbauer spectra

In the Figs. 4 and 5 Mössbauer spectra for LF sample and for both series of mixed oxides MF and TF are presented, respectively.

Table 3
Unit cell parameters of mechanochemicaly treated and annealed at 1000 °C/10 h samples

Nominal composition		Mechanochemicaly treated	Annealed at 1000 °C
TM (50:50)	a (Å)	3.949 (3)	5.566 (4)
	b		5.552 (5)
	c		7.871 (6)
	V (Å^3)	61.6 (2)	243.2 (2)
MF (40:20)	a (Å)	3.936 (1)	5.563 (2)
	b		5.557 (2)
	c		7.861 (2)
	V (Å^3)	60.97 (6)	243.0 (1)
MF (30:27)	a (Å)	3.9355 (9)	5.549 (4)
	b		5.551 (5)
	c		7.854 (6)
	V (Å^3)	60.95 (4)	241.9 (3)
MF (20:34)	a (Å)	3.933 (2)	5.557 (3)
	b		5.548 (4)
	c		7.855 (5)
	V (Å^3)	60.83 (8)	242.2 (2)
MF (10:40)	a (Å)	3.933 (2)	5.559 (3)
	b		5.552 (2)
	c		7.860 (2)
	V (Å^3)	60.83 (8)	242.6 (1)
TF (40:13)	a (Å)	3.934 (2)	5.565 (1)
	b		5.559 (1)
	c		7.867 (3)
	V (Å^3)	60.89 (8)	243.4 (1)
TF (30:27)	a (Å)	3.936 (2)	5.563 (2)
	b		5.557 (2)
	c		7.863 (1)
	V (Å^3)	60.96 (9)	242.1 (1)
TF (20:40)	a (Å)	3.938 (2)	5.561 (3)
	b		5.557 (2)
	c		7.848 (6)
	V (Å^3)	61.07 (9)	242.5 (2)
TF (10:53)	a (Å)	3.919 (3)	5.560 (3)
	b		5.559 (2)
	c		7.850 (4)
	V (Å^3)	60.2 (2)	242.6 (2)
LF	a (Å)	3.931 (2)	5.553 (3)
	b		5.550 (2)
	c		7.858 (5)
	V (Å^3)	60.75 (8)	242.2 (2)

The Mössbauer parameters of all samples are presented in Table 5.

The Mössbauer spectrum of sample LF consists of a single sextet with narrow lines with parameters (IS = 0.37 mm/s, QS = −0.03 mm/s and H_{eff} = 52.4 T) typical of Fe^{3+}-ions in octahedral coordination. The value of the hyperfine magnetic field is closer to that found by Eibschütz [38] for a bulk well-crystallized LF obtained by conventional heating. The spectrum of LF formed by mechanical milling included lines of sextet spectrum with H_{eff} = 48.9 T [39].

The Mössbauer spectra of samples MF (40:20), MF (30:27), MF (20:34), MF (10:40), TF (40:13), TF (30:27), TF (20:40) are similar – they are quadrupole doublets due to Fe^{3+} ions in a high spin and octahedral coordination. Values of quadrupole splitting exhibit a tendency to increase with decreasing Fe concentration (Table 5) but the difference is small. IS of spectra of samples TF (40:13), TF (30:27), TF (20:40) and doublet of TF (10:53) is lower as compared to those of samples with varied Mg content.

As shown in Fig. 5 the spectrum of sample TF (10:53) consists of a sextet with a relatively wide lines and doublet compound. The sextet component has a lower hyperfine field value (H_{eff} = 50.2 T) and broader lines than that for LF sample. This effect can be related to the different configurations of Fe^{3+} due to the presence of Ti and Mg in M position. The doublet component is due to high spin Fe^{3+}-ions in octahedral coordination.

In the sample TF (10:53) two-component spectrum is registered. In this case the presence of two components – sextet and doublet, can be considered as a differentiation of areas with different iron content. In the areas ''richer'' in Fe due to exchange interactions a sextet appears in the spectrum. Substitution of a nonmagnetic ions (Ti, Mg) for the magnetic one (Fe) will tend to dilute the magnetic coupling between iron ions and will tend to reduce the magnetic transition temperature. This substitution weakens the long-range magnetic interactions. The decrease of Fe content in the samples below 0.53 reduces the number of Fe^{3+}–O^{2-}–Fe^{3+} interactions and the recorded spectra show no hyperfine magnetic structure, i.e. the spectra comprise doublets.

3.5. XPS analysis

The binding energies of O 1s, La $3d_{5/2}$, Ti $2p_{3/2}$, Fe $2p_{3/2}$ and Mg 2p core levels are summarized in Table 6.

Energy position of La 3d corresponds to La^{3+} in La_2O_3. The Ti 2p peak position is within the interval 456.9–458.4 eV and may be attributed to photoemission from Ti^{3+} ions whose binding energy varies due to the difference in the unit cell parameters. The binding energy of Mg 2p level is close to 49 eV, which corresponds to the Mg^0 state. The low BE values of Mg 2p and Mg 1s peaks indicate that the electron density around Mg atoms increased due to charge redistribution between the metal ions in the perovskite structure. This is consistent with the same observation for the NiMg alloys [40] and Pd supported catalysts [41]. The Fe $2p_{3/2}$ and O 1s level spectra of both series of catalysts are presented in Figs. 6 and 7, respectively. The binding energy for Fe $2p_{3/2}$ is characteristic for Fe^{2+} (samples MF (40:20), MF (30:27), MF (20:34), TF (30:27) and TF (10:53)) and of Fe^{3+} (samples MF (10:40), TF (40:13) and TF (20:40)). From these results it appears that in the surface layers of all samples the iron is partially reduced during the annealing in the air at 1000 °C.

The O 1s XPS spectra of LF show one large peak, without clear pronounced peak maxima. For the both series of substituted samples the O 1s XPS spectra show two main peaks at 528.5–529.6 eV ascribed to regular lattice oxygen and 530.6–531.8 eV assigned to adsorbed oxygen species as well as to hydroxyl (OH^-) and carbonate (CO_3^{2-}) species. Interesting

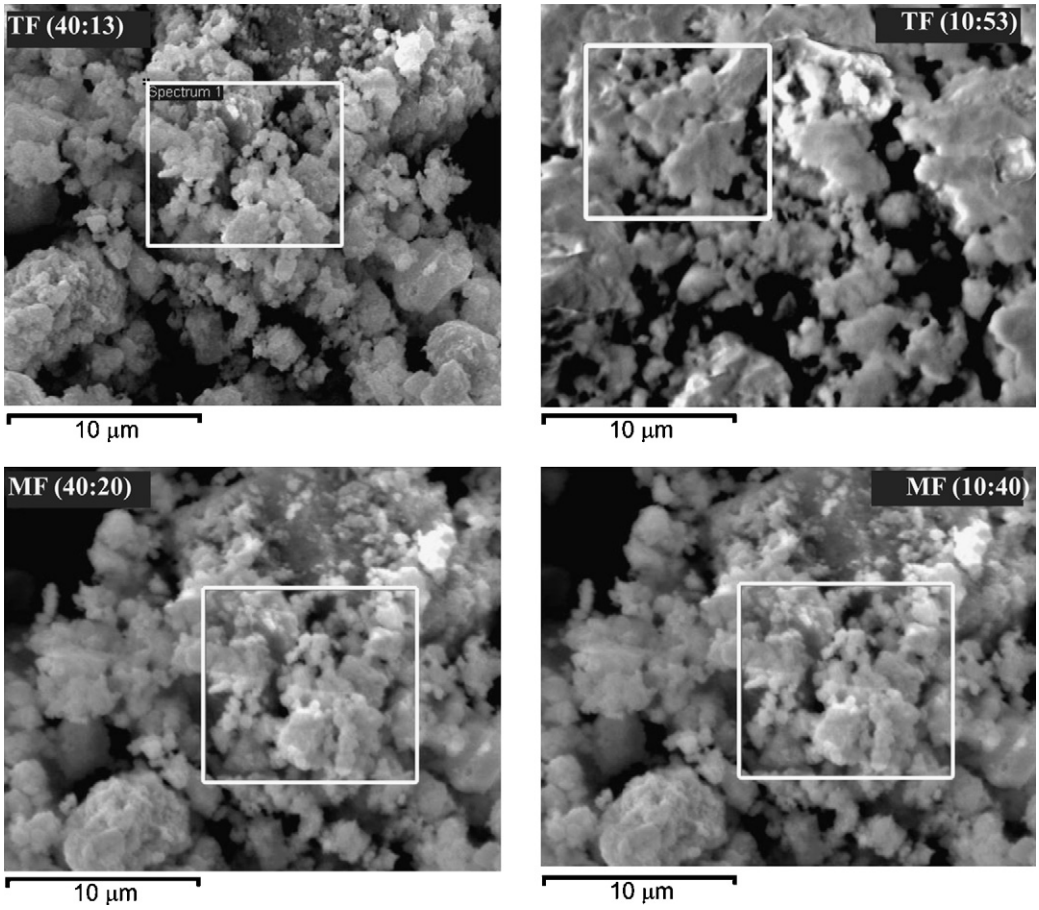

Fig. 3. SEM images for the samples with lowest and highest degree of substitution. Selected region was used for EDS analysis.

Table 4
The nominal atomic ratios (sum = La + Ti + Mg + Fe) and the atomic ratios obtained by EDS, as well as grain size for samples with lowest and highest degree of substitution

Sample	La/sum		Ti/sum		Mg/sum		Fe/sum		Grain size (μm)
	Nom.	EDS	Nom.	EDS	Nom.	EDS	Nom.	EDS	
MF (40:20)	0.50	0.48	0.21	0.20	0.20	0.22	0.10	0.09	0.34
MF (10:40)	0.50	0.52	0.20	0.21	0.05	0.06	0.20	0.20	0.48
TF (40:13)	0.50	0.45	0.20	0.23	0.25	0.24	0.07	0.07	0.42
TF (10:53)	0.50	0.43	0.05	0.04	0.25	0.30	0.26	0.23	0.58

result of XPS is higher population of adsorbed species on the surface of TF series in respect to that of the series MF.

The results revealed that both Ti and Fe exist at the surface of the samples in different valence state, namely Ti^{3+} and Ti^{4+} and Fe^{3+} and Fe^{2+}. The partial reduction of Ti^{4+} to Ti^{3+} was observed even in the bulk of TM (50:50) synthesized at high temperature under pressure in air [42].

In Fig. 8, plots of the intensity determined by XPS for each element, normalized to the sum of La + Ti + Mg + Fe intensities, are represented. This representation allows one to eliminate the O 1s and C 1s participation and their possible surface segregation.

Comparing these plots the several observations could be made. The surface composition of both series of perovskite

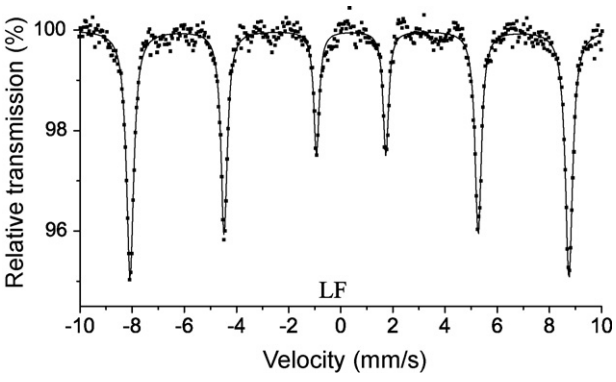

Fig. 4. Mössbauer spectrum of LF sample.

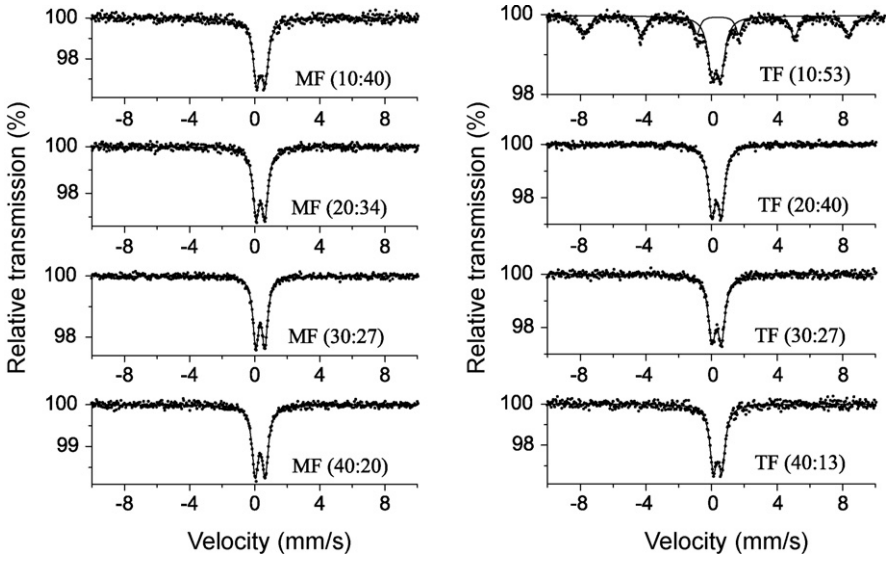

Fig. 5. Mössbauer spectra of MF and TF series of samples.

departs considerably from the nominal value. In the both series a significant decrease in La/sum ratio at surface in respect to the bulk was observed (Fig. 8a). This decrease remains fairly constant throughout the series TF, while for the MF series La/sum ratio increases with Fe content and almost reaches the nominal value for the sample MF (10:40). Mg/sum ratio (Fig. 8b) for the samples with constant nominal content of Mg, i.e. for the TF series, is significantly higher, while the Ti/sum ratio (Fig. 8c) is something lower in respect to that in the bulk. However, for all samples in MF series both Mg/sum and Ti/sum ratios are higher than nominal. Fe/sum ratio (Fig. 8d) is lover than nominal for all members of the both series and does not increase monotonously with Fe content. Consequently, in all samples of a series TF, significant segregation of Mg to the

Table 5
Mössbauer parameters of the obtained perovskite samples

Sample	Compounds	IS (mm/s)	QS (mm/s)	H_{eff} (T)	FWHM (mm/s)	G (%)
MF (40:20)	Db–Fe^{3+}	0.34	0.61	–	0.56	100
MF (30:27)	Db–Fe^{3+}	0.34	0.56	–	0.50	100
MF (20:34)	Db–Fe^{3+}	0.35	0.54	–	0.47	100
MF (10:40)	Db–Fe^{3+}	0.35	0.53	–	0.51	100
TF (40:13)	Db–Fe^{3+}	0.32	0.62	–	0.59	100
TF (30:27)	Db–Fe^{3+}	0.32	0.59	–	0.52	100
TF (20:40)	Db–Fe^{3+}	0.31	0.57	–	0.52	100
TF (10:53)	Sx–Fe^{3+}	0.34	−0.04	50.2	0.45	53
	Db–Fe^{3+}	0.30	0.55	–	0.62	47
LF	Sx–Fe^{3+}	0.37	−0.03	52.4	0.30	100

IS – isomer shift relative to metallic α-Fe at room temperature. QS – quadrupole splitting for doublets or quadrupole shift for sextets. H_{eff} – effective magnetic field. Estimated standard deviations are <1% for G, <0.1 T for H_{eff} and 0.01 for the other parameters.

Table 6
XPS binding energies (eV) of photoelectron peaks in the synthesized perovskite samples

Sample	O 1s	La $3d_{5/2}$	Ti $2p_{3/2}$	Fe $2p_{3/2}$	Mg 2p
TM (50:50)	529.1, 531.0	833.6	457.4	–	48.6
MF (40:20)	528.5, 530.6	832.6	457.0	709.0	48.3
MF (30:27)	528.8, 531.0	833.0	457.1	709.2	48.2
MF (20:34)	528.6, 530.5	832.4	456.9	708.9	48.5
MF (10:40)	529.6, 531.3	834.2	458.0	710.5	48.6
TF (40:13)	528.6, 531.3	833.4	457.1	709.3	49.3
TF (30:27)	529.6, 531.8	834.8	458.4	710.9	49.4
TF (20:40)	528.4, 530.9	832.8	457.0	709.2	48.4
TF (10:53)	528.6, 531.0	833.2	457.2	710.0	48.8
LF	529.5, 531.8	833.8	–	710.3	–

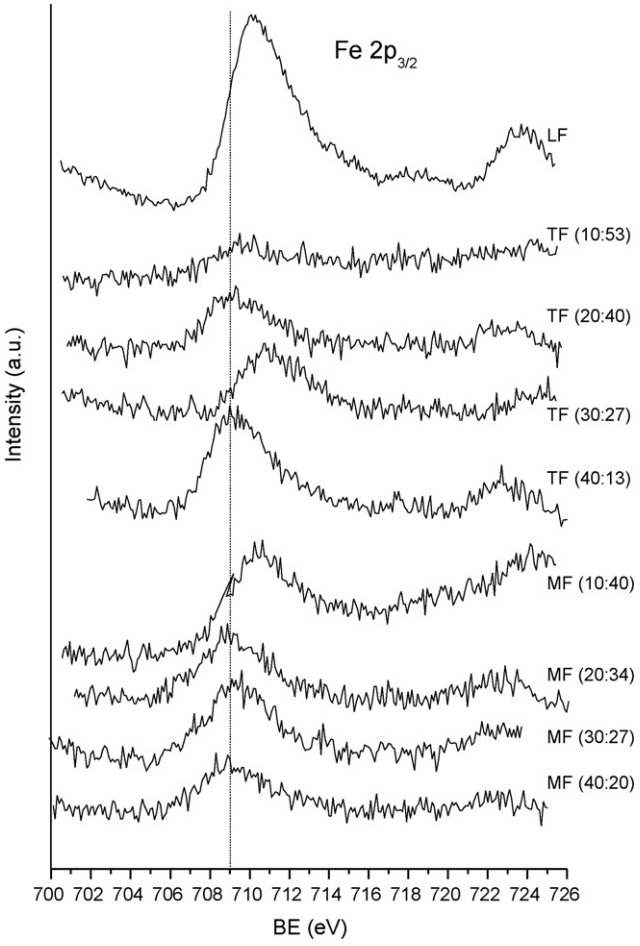

Fig. 6. Fe $2p_{3/2}$ core-level spectra for synthesized perovskite samples.

surface was observed, while in the series MF concurrent enrichment of surface with Mg and Ti is observed.

3.6. TPD

Oxygen desorption curves for all investigated samples are presented in Fig. 9.

As it is seen from the Fig. 9 the evaluation of oxygen from sample TM (50:50) which was detected by mass spectroscopy takes place at 700 °C. For LF sample and both series of iron containing samples two broadened low temperature peaks below 700 °C were observed. The first peak with onset temperature at 200 °C (or centered at about 300 °C) is more intense for the samples of the series TF. The exception is the sample TF (40:13). The second very large peak with onset temperature at 350 °C (or centered about 500 °C) is more pronounced for LF sample and for all samples of the series MF. It looks that the intensity of both peaks increases with the degree of Fe substitution. The existence of two peaks at lower temperature (α state) can be attributed to the various kinds of adsorbed oxygen. The peak with onset temperature between 700 and 750 °C is observed in all investigated samples and is characteristic for desorption of the lattice oxygen from perovskites (β state).

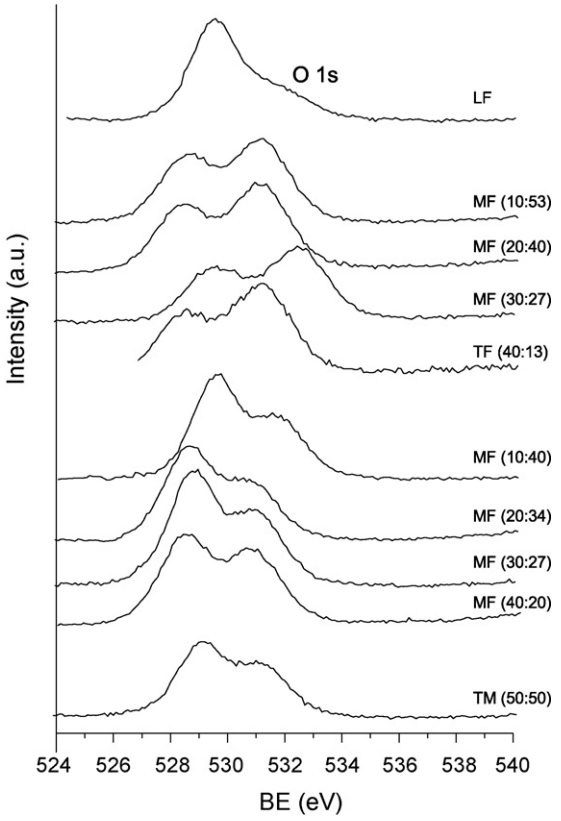

Fig. 7. O 1s core level spectra for synthesized perovskite samples.

The water desorption peak for the sample TM (50:50) and for all Fe substituted samples show a large tail which is extended to the temperature of 400 °C. This result suggests the difficulty to eliminate OH-groups adsorbed at La, Mg particularly Ti atoms [43].

3.7. Catalytic activity

Methane oxidation activity data expressed as percent of CH_4 conversion as a function of temperature for all synthesized samples presented in Fig. 10, are obtained using the same catalyst weight. Since their SSA are close (2–3 m^2/g), it was possible to compare activity according the conversion of methane.

From these plots it is evident that activity is higher for the samples of TF series in respect to the samples of MF series with similar substitution degree of Fe. Sample $LaFeO_3$ (LF) shows higher activity at low temperatures (up to 550 °C) in respect to Mg and Ti substituted samples. However, almost no increase of activity was observed in the temperature range from 700 to 800° C. With further increase of temperature activity of LF increases sharply. Temperature seems to play an important role in used reaction conditions, perhaps in modification of surface properties of catalyst $LaFeO_3$ which may reflect the alteration of the bulk availability of α and β oxygen [15].

In order to check the stability of samples under reaction conditions the measurements of methane conversion are performed during the heating and cooling, and for chosen samples presented in Fig. 11.

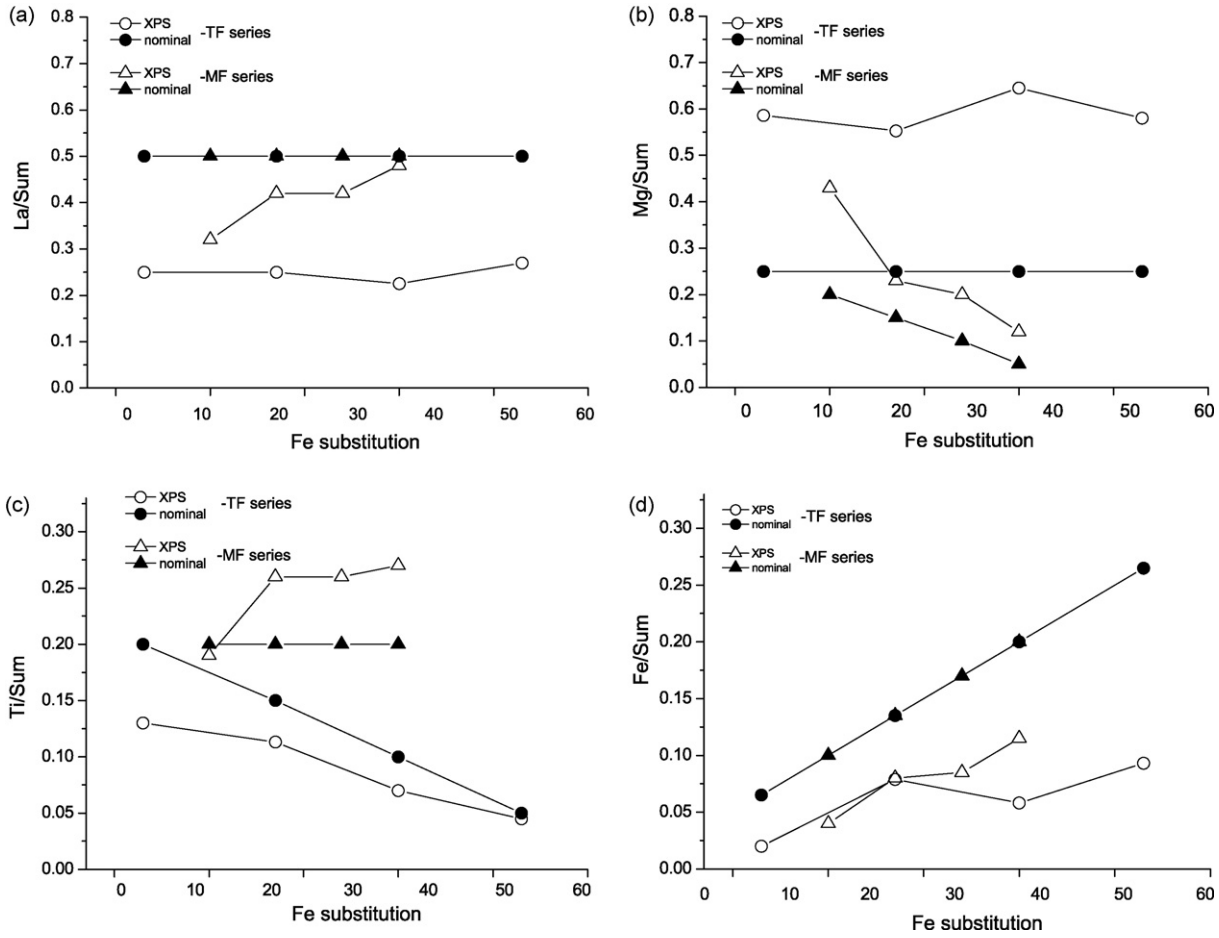

Fig. 8. Plot of the intensity of (a) La; (b) Mg; (c) Ti and (d) Fe element normalized to the sum of the intensities of the elements at the surface (XPS) and in the bulk (nominal) as a function of substitution degree.

In contrast to the results obtained for LF sample no decrease of activity was obtained over both series of catalyst. The data of catalytic tests are reproductive in three runs.

Temperatures necessary to give the conversions of T_{10}, T_{30}, T_{50} and T_{80} as a function of Fe content for MF and TF series are presented in Fig. 12a and b, respectively.

For MF series (Fig. 12a) the temperature necessary to give T_{10} decreases with the Fe content in the whole investigated range, but the temperatures for T_{30}, T_{50} and T_{80} show a maximum for the MF (30:27). The fact could be explained in the hypothesis that some other factors as nonstoichiometry and crystalline defects may contribute to higher activity of MT (40:20) sample. In the case of the TF series (Fig. 12b) the temperatures for T_{10}, T_{30}, T_{50} and T_{80} decreases with the Fe content in all investigated Fe range. Slight changes of temperatures with increasing the Fe content observed in both series of catalysts implies that the catalytic activity is not significantly correlated to the Fe content.

The temperatures for T_{10}, T_{30}, T_{50} and T_{80} were always about 80 °C lower for the TF series than those attended for the MF samples with same or very close to the Fe content.

4. Discussion

The comparison of catalytic performance in terms of conversion in the function of reaction temperature (Fig. 10) or the half conversion temperatures as a function of the Fe content (Fig. 12) indicates that each sample from the TF series poses a higher activity in respect to the all samples of the MF with similar degree of Fe substitution. A relevant factor to consider when assigning the sites responsible for catalytic activity is the phase composition of perovskite samples obtained by used preparation method. X-ray powder diffraction data show that after annealing of precursor at 1000 °C almost single-phase samples were formed with orthorhombic perovskite-type structures and a high degree of crystallinity. The traces of La_2O_3 phase are presented in some perovskite samples (Fig. 2). A slight difference in unit cell parameters observed within each group of perovskites and consequently in unit cell volumes could be a result of different ratios of elements in the octahedral site and their valence states [44] as well as the formation of vacancies at all sites and the consequence of a distortion of octahedral alignment of the atom in B position.

TPD pattern (Fig. 9) of TM (50:50) show only desorption peak with onset temperature of 700 °C which is ascribed to the

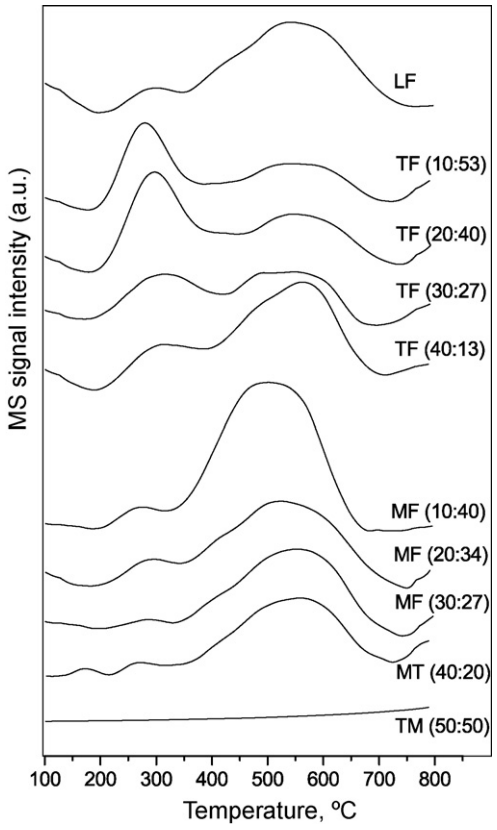

Fig. 9. TPD–MS spectra of oxygen evaluation for synthesized perovskite-type samples (see Table 2 for details).

evaluation of lattice oxygen. However, TPD patterns of Fe substituted samples besides the high temperature peak, show two broad peaks at lower temperature, whose relative intensities seems to increase with the degree of substitution of Ti or Mg by Fe. Evidently, for TF series the oxygen adsorption sites were different from those of MF series, resulting in different catalytic behavior. Upon substitution of Ti^{4+} by Fe^{3+} or the Mg^{2+} by Fe^{3+} charge compensation can be

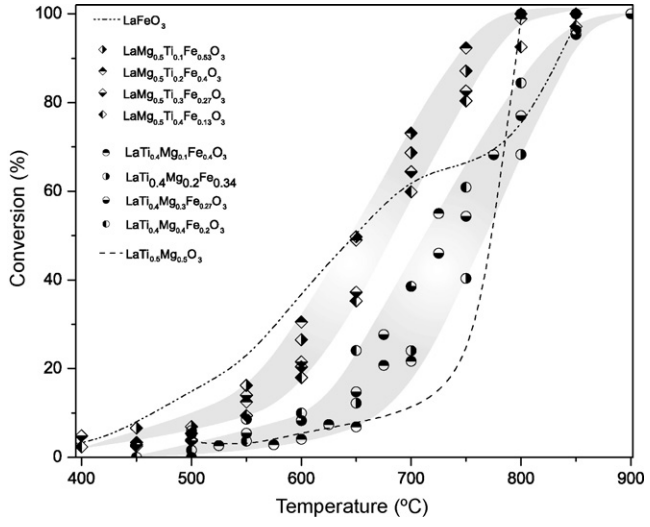

Fig. 10. CH_4 conversion as a function of temperature for the perovskite-type samples of both series.

achieved by change of oxidation state of Ti and Fe ions and/or creation of oxygen and cation vacancies. However, it is possible that Ti changes oxidation state between $Ti^{3+}$and Ti^{4+}.

Numerous experimental data available in literature indicate that only noble metals and transition metal oxides show reasonable activity in deep oxidation of hydrocarbons. The order of activity seems to correlate with the strength of metal–oxygen bond [45]. The results of the present investigations clearly show that the activity of perovskite in methane deep oxidation increases in the order TM (50:50) < MF series < TF series. This is in accordance with the decrease of temperature of oxygen desorption peaks.

Consequently, higher activity of the TF series samples probably could be related to the presence of predominantly most labile oxygen species evidenced by TPD at lowest temperature of oxygen evaluation. It looks that adsorbed oxygen mainly participated in reaction at lower temperatures. In support of this XPS revealed significantly higher population of adsorbed oxygen at the surface of all samples of TF series than in MF series of samples. However, predominant oxygen evaluation evidenced by TPD at higher temperature from the MF series samples require higher temperatures to start reacting and thus limiting to some extent the overall activity of the samples. The $LaTi_{0.5}Mg_{0.5}$ O_3 (TM) sample is almost inactive to the temperature of 700 °C with sharp increase in activity with further increase of temperature.

Deactivation of catalysts is negligible up to 800 °C, as reported in Fig. 11. The exception is LF sample. As often reported in literature the Fe^{3+} incorporated in perovskite structure reduces to Fe^{2+} at higher temperatures than in iron oxides and this reduction does not change the basic perovskite structure. According TPR data Ciambelli et al. [11] show that low extent of iron is reduced in $LaFe_{1-x}Mg_xO_3$ compared to other metal cations, namely manganese and cobalt in lanthanum based perovskites. Consequently, they concluded that Fe^{3+} is less easily reducible when an alkaline earth cation, such as Mg, partly occupies the octahedral B sites. Merino et al. [46] reported that Fe in $LaCo_{1-x}Fe_xO_3$ plays the important role in preservation of perovskite structure preventing the segregation and total reduction of Co in deep oxidation of ethanol and propane. Ponce et al. [9] found that activity of $La_{1-x}Sr_xMnO_3$ in methane oxidation is mainly determined by stability of Mn^{4+} in perovskite structure towards reduction. According to the previous articles the thermal stability of investigated perovskite samples can be probably ascribed to unchanged content of iron centers supposed to be active sites.

Another important parameter to be considered is the surface composition revealed by XPS. According to EDS analysis the distribution of elements in the bulk is almost homogeneous (Table 4). However, XPS show that in all samples of a series TF, important segregation of Mg to the surface was observed, while in the series MF concurrent enrichment of surface with Mg and Ti is found. Data of Mössbauer spectroscopy of all studied samples identify Fe^{3+} in octahedral coordination. Moreover, according the XPS Fe in the surface layers of all samples is partially reduced to Fe^{2+} valence state. The increase of catalytic activity in propane oxidation of $La_{1-x}Ce_xFeO_3$ with $x \leq 0.1$,

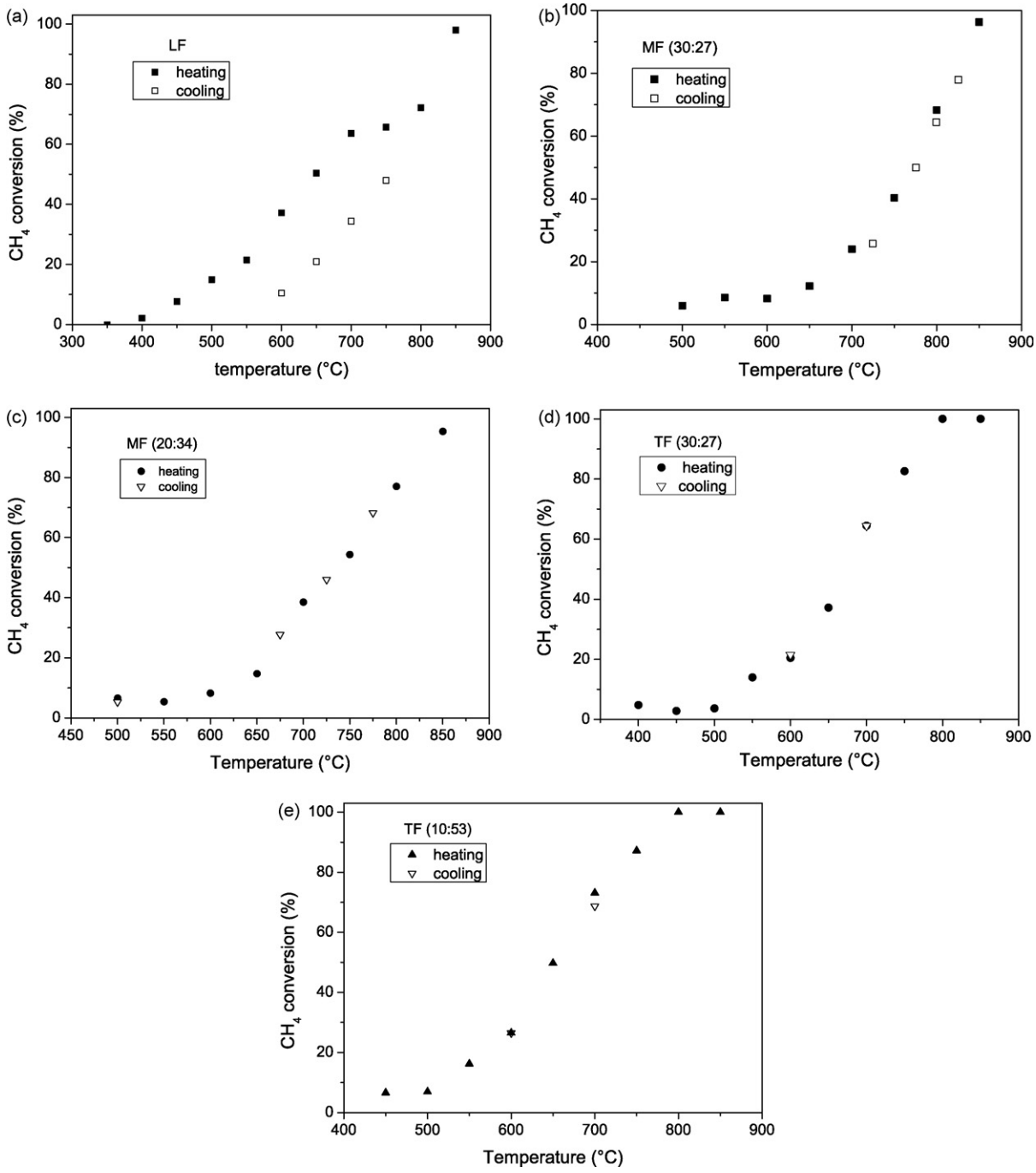

Fig. 11. CH_4 conversion during heating and cooling: (a) LF; (b) MF (30:27); (c) MF (20:34); (d) TF (30:27) and (e) TF (10:53).

where a separate CeO_2 phase was apparent, Nitadori et al. [47] ascribed to the presence of Fe^{2+} ions in the solid. According to the previous the thermal stability of catalysts is related to the phase stability of the active component and probably in our case can be ascribed to fluctuation between two stable oxidation states, Fe^{2+} and Fe^{3+}.

The degrees of Ti or Mg substitution for Fe are close in both series of catalyst. It is important to note that the activities of the both series are not related significantly to the Fe content in the bulk (Figs. 10 and 12). XPS show that Fe/sum ratio is significantly lower than the nominal one (Fig. 8d). This result implies that Fe does not segregate towards the surface in all investigated samples and that the surface layers of α-Fe_2O_3 were not formed even in the sample with the highest Fe content, because hematite is almost inactive, due to less favored oxygen adsorption [17]. Thus the surface structure differs substantially from the bulk composition and may significantly influence methane oxidation activity.

The presence of Mg with stable valence and Ti and Fe which potentially assume different oxidation states in B position makes very difficult to understand real cause of enhanced activity of the samples with constant content of Mg.

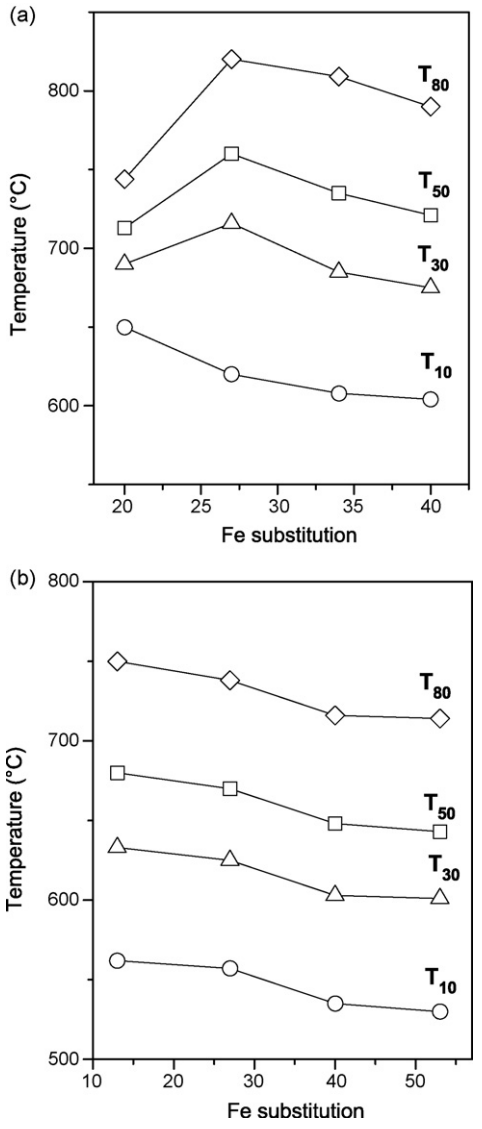

Fig. 12. T_{10}, T_{30}, T_{50}, and T_{80} as a function of Fe substitution: (a) MF series, (b) TF series.

5. Conclusions

Mechanochemical activation was used to prepare the precursor of following mixed oxides: $LaTi_{0.4}Mg_yFe_xO_3$ ($0.2 \leq x \leq 0.4$; $0.1 \leq y \leq 0.4$), (denoted as MF series) and $LaMg_{0.5}Ti_yFe_xO_3$ ($0.13 \leq x \leq 0.53$; $0.1 \leq y \leq 0.4$), (denoted as TF series), $LaFeO_3$ (LF sample) and $LaTi_{0.5}Mg_{0.5}O_3$ (TM (50:50) sample). The precursor was annealed at 1000 °C in air. After annealing all synthesized samples were almost single perovskite phase, with trace amounts of La_2O_3. EDS show that the distribution of elements in the bulk is almost homogeneous. Data of Mössbauer spectra of all studied samples identify Fe^{3+} in octahedral coordination. The results of present investigations clearly show that activity of perovskite in the methane deep oxidation increases in the order TM (50:50) < MF series < TF series. The TF samples are more active as compared to the samples MF with similar Fe content. Higher activity of the samples with constant content of Mg in B position of TF series probably could be related to the presence of predominantly most labile oxygen species evidenced by TPD at lowest temperature of oxygen evaluation. Consequently, more strongly bond oxygen found in MF series required higher temperatures to start reacting and thus limiting to some extent the overall activity. The surface composition differs to an important extent from the bulk composition and also may affect the catalytic activity. The Fe substituted perovskite are thermal stable in used experimental conditions of methane oxidation up to the temperature of 850 °C. The thermal stability of catalysts is related to the phase stability of the active component and probably in our case can be ascribed to fluctuation between two stable oxidation states of iron, Fe^{2+} and Fe^{3+}.

Acknowledgements

This project was supported by the Grant Nos. 142019 B and 142030 B from the Ministry for Science of the Republic of Serbia.

References

[1] R.J.H. Voorhoeve, J.P. Remeika, P.E. Freeland, B.T. Matthias, Science 177 (1972) 353.
[2] T. Seiyama, in: J.G.L. Fierro (Ed.), Properties, Application of Perovskite-type Oxides, Marcel Dekker, New York, 1993, , Chap. 10.
[3] J.M.D. Tascon, S. Mendioroz, L.G. Tejuca, J. Phys. Chem. 124 (1981) 109.
[4] H. Arad, T. Yamada, K. Eguchi, T. Seiyama, Appl. Catal. 26 (1986) 265.
[5] V.C. Belessi, P.N. Trikalitis, A.K. Ladavos, T.V. Bakas, P.J. Pomonis, Appl. Catal. A: Gen. 177 (1999) 53.
[6] P.D. Fagg, V.V. Kharton, J.R. Frade, A.A.L. Ferreira, Solid State Ion. 156 (2003) 45.
[7] A.L. Sauvinet, J. Fouletier, F. Gaillard, M. Primet, J. Catal. 209 (2002) 25.
[8] P. Ciambelli, S. Cimino, G. Lasorella, L. Lisi, S. De Rossi, M. Faticanti, G. Minelli, P. Porta, Appl. Catal. B: Environ. 37 (2002) 231.
[9] S. Ponce, M.A. Peňa, J.L.G. Fierro, Appl. Catal. B: Environ. 24 (2000) 193.
[10] P. Porta, S. Cimino, S. De Rossi, M. Faticanti, G. Minelli, I. Pettiti, Mater. Chem. Phys. 71 (2001) 165.
[11] P. Ciambelli, S. Cimino, S. De Rossi, L. Lisi, G. Minelli, P. Porta, G. Russo, Appl. Catal. B: Environ. 29 (2001) 239.
[12] P. Ciambelli, S. Cimino, L. Lisi, M. Faticanti, G. Minelli, I. Pettiti, P. Porta, Appl. Catal. B: Environ. 33 (2001) 193.
[13] L. Forni, I. Rossetti, Appl. Catal. B: Environ. 38 (2002) 29.
[14] N.A. Merino, B.P. Barbero, P. Ruiz, L.E. Cadús, J. Catal. 240 (2006) 245.
[15] R. Spinicci, A. Tofanari, A. Delmastro, D. Mazza, S. Ronchetti, Mater. Chem. Phys. 76 (2002) 20.
[16] V.C. Belessi, A.K. Lavados, P.J. Pomonis, Appl. Catal. B: Environ. 31 (2001) 183.
[17] A. Delmastro, D. Mazza, S. Ronchetti, M. Vallino, R. Spinicci, P. Brovetto, M. Salis, Matter. Sci. Eng. B 79 (2001) 140.
[18] V.C. Belessi, C.N. Costa, T.V. Bakas, T. Anastasiadou, P.J. Pomonis, A.M. Efstahou, Catal. Today 59 (2000) 347.
[19] S.R. Jain, K.C. Adiga, V.R.P. Verneker, Combust. Flame 40 (1981) 71.
[20] D.A. Fumo, M.R. Morelli, A.M. Segadăes, Mater. Res. Bull. 51 (1996) 1243.
[21] A. Civera, M. Paavese, G. Saracco, V. Soecchia, Catal. Today 83 (2003) 199.
[22] A. Civera, G. Negro, S. Specchia, G. Saracco, V. Specchia, Catal. Today 100 (2005) 275.
[23] E. Gaffet, G. Le Caër, in: H.S. Nalwa (Ed.), Encyclopedia of Nanoscience and Nanotechnology, vol. 10, American Scientific, Stevenson Ranch, CA, 2004, p. 1.

[24] S. Kaliaguine, A. Van Neste, V. Szabo, J.E. Galot, M. Bassir, R. Muzychyuk, App. Catal. A: Gen. 209 (2001) 345.
[25] V. Szabo, M. Bassir, A. Van Neste, S. Kaliaguine, Appl. Catal. B: Environ. 37 (2002) 175.
[26] V. Szabo, M. Bassir, J.E. Gallot, A. Van Neste, S. Kaliaguine, Appl. Catal. B: Environ. 42 (2003) 265.
[27] V. Szabo, M. Bassir, A. Van Neste, S. Kaliaguine, Appl. Catal. B: Environ. 43 (2003) 81.
[28] S. Petrović, P. Kirilov-Stefaniv, Lj. Karanović, M. Zdujić, A. Terlecki-Baričević, Mater. Sci. Forum 453–454 (2004) 417.
[29] S. Petrović, P. Kirilov-Stefaniv, Lj. Karanović, M. Zdujić, A. Terlecki-Baričević, Appl. Catal. B: Environ. 58 (2005) 133.
[30] L.G. Garvey, Powder Diff. 1 (1986) 114.
[31] A. Meden, M. Čeh, Mater. Sci. Forum 278–281 (1998) 773.
[32] M.P. Crosnier-Lopez, H. Duroy, Y. Calage, J.M. Greneche, J.L. Fourquet, Mater. Res. Bull. 36 (2001) 651.
[33] M. Marezio, P.D. Dernier, Mater. Res. Bull. 6 (1971) 23.
[34] T.A. Vanderah, V.L. Miller, I. Levin, S.M. Bell, T.J. Negas, Solid State Chem. 177 (2004) 2023.
[35] R. Ubic, Y. Hu, I. Abrahams, Acta Crystallogr. B62 (2006) 52.
[36] M.W. Lufaso, P.W. Barnes, P.M. Woodward, Acta Crystallogr. B62 (2006) 397.
[37] M. Alifanti, J. Kirchnerova, B. Delmon, D. Klvana, Appl. Catal. A: Gen. 262 (2004) 167.
[38] M. Eibschütz, S. Shtrikman, D. Treves, Phys. Rev. 156 (1967) 562.
[39] F.J. Berry, X. Ren, J.R. Gancedo, J.F. Marco, Hyperfine Interact. 156–157 (2004) 335.
[40] C. Iwakura, H. Inoue, S.G. Zhang, S. Nahara, J. Alloy Compd. 653 (1999) 293.
[41] T.H. Fleisch, R.F. Hicks, A.T. Bell, J. Catal. 87 (1984) 398.
[42] J.P. Miao, L.P. Li, Y.B. Song, D.P. Xu, Z. Lu, W.H. Su, Mater. Chem. Phys. 62 (2000) 226.
[43] A. Glisenti, J. Mol. Catal. A: Chem. 153 (2000) 169.
[44] E.R. Kirkoech, F. Azough, R. Freer, J. Am. Chem. Soc. 88 (2005) 768.
[45] Y. Morooka, A. Ozaki, J. Catal. 5 (1966) 116.
[46] N.A. Merino, B.P. Barbero, P. Ruiz, L.E. Cadu's, J. Catal. 240 (2006) 245.
[47] T. Nitadori, M. Misono, J. Catal. 93 (1985) 459.